Supporting Information

Enhanced H_2 gas sensing properties of Au@In_2O_3 core-shell hybrid metal-semiconductor heteronanostructures

Rama Krishna Chava[a], Sang-Yeob Oh[b] and Yeon-Tae Yu[a]*

[a]Division of Advanced Materials Engineering and Research Centre for Advanced Materials Development, College of Engineering, Chonbuk National University, Jeonju 561-756, South Korea.

[b]Korea Institute of Carbon Convergence Technology, 110-11, Banryong-ro, Deokjin-gu, Jeonju, 561-844, South Korea

*E-mail: yeontae@jbnu.ac.kr

Synthesis of In_2O_3 Nanoparticles:

In_2O_3 nanoparticles are synthesized by using hydrothermal method and basic idea was taken from the reported literature. [1] The solution containing 2 mm of Na_3Cit and 2.4 mm of $InCl_3$ was kept under stirring. The solution was stirred at room temperature for 30 minutes and then 2 mm of Urea was added and kept on stirring for another 30 minutes. After being stirred for 30 minutes the transparent solution was transformed into a 50 ml Teflon lined stainless steel autoclave and was heated at 140 ^oC for 18 hours. Then autoclave was cooled to room temperature naturally. The obtained white precipitate was washed and centrifuged with de ionized water at 9000 rpm and repeated the purification and centrifugation five times. The obtained sample was dried at 60 ^oC for overnight so as to obtain the Indium Hydroxide spherical nanoparticles. In_2O_3 spherical NPs were obtained by calcining the Indium hydroxide spherical nanoparticles synthesized in the above manner at 350 ^oC for 2 hours. The heating rate was controlled at 2 ^oC per minute.

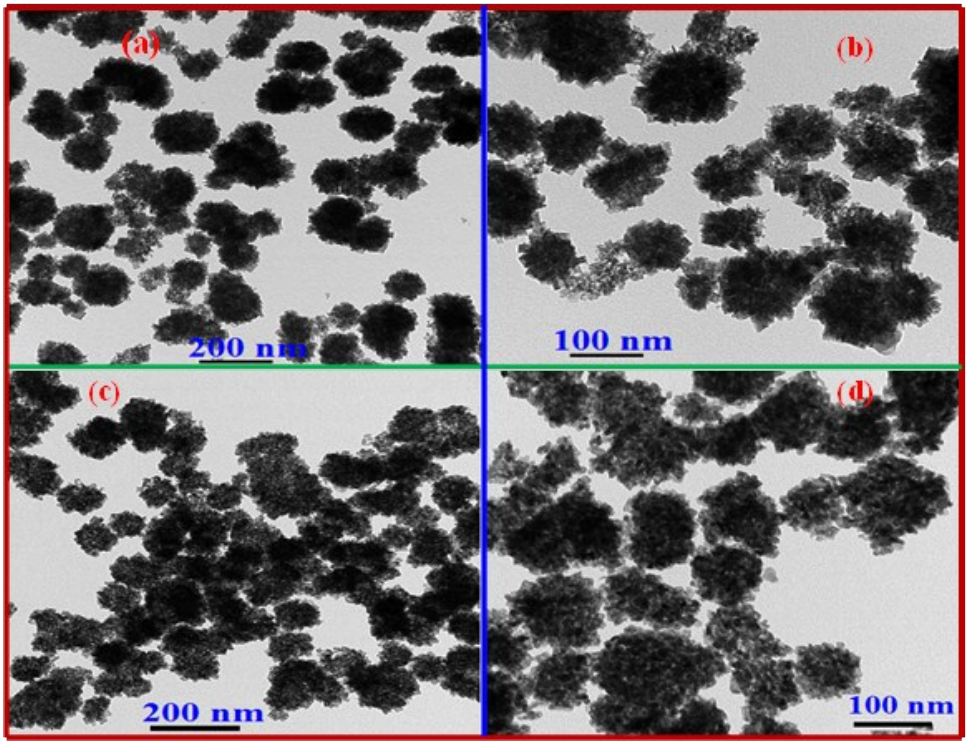

Figure S1: TEM images of $In(OH)_3$ (a, b) and In_2O_3 (c, d) NPs.

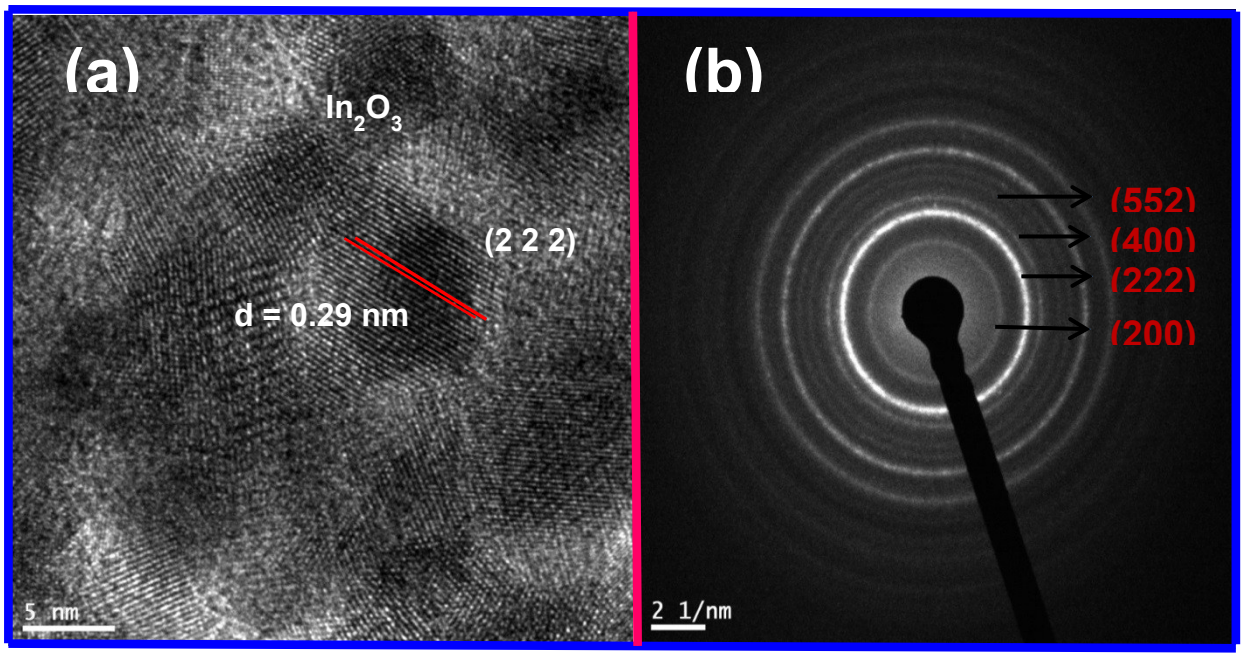

Figure S2: HR-TEM image (a) and SAED patterns (b) of In_2O_3 NPs.

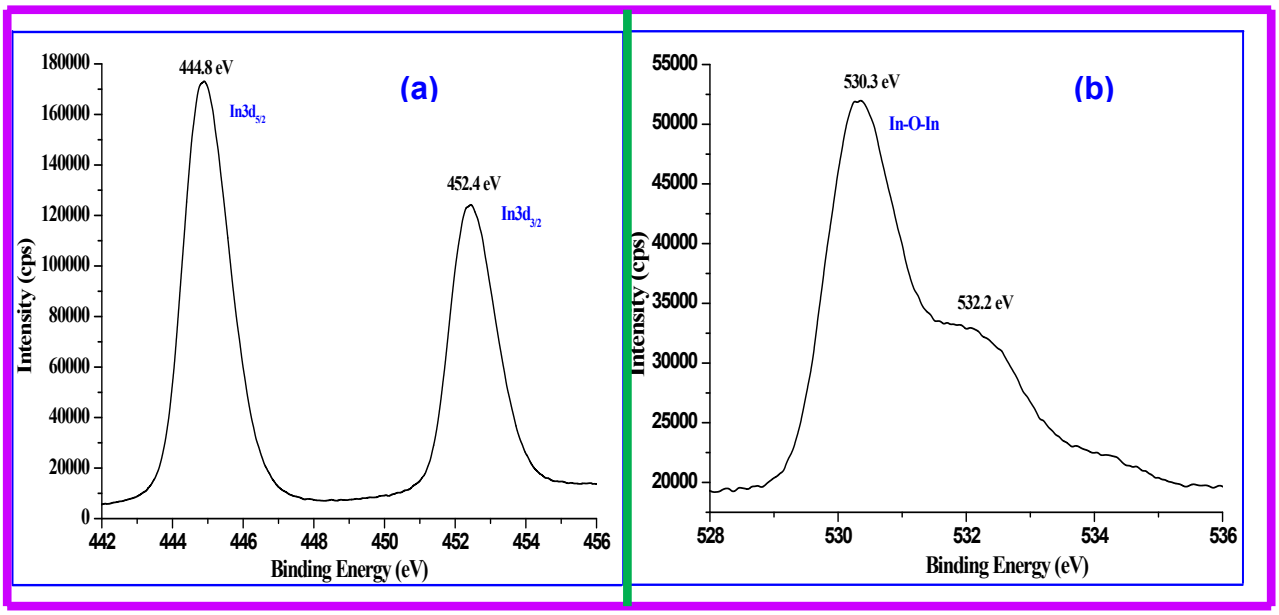

Figure S3: XPS Spectra of (a) In 3d and (b) O1s elements in In_2O_3 NPs.

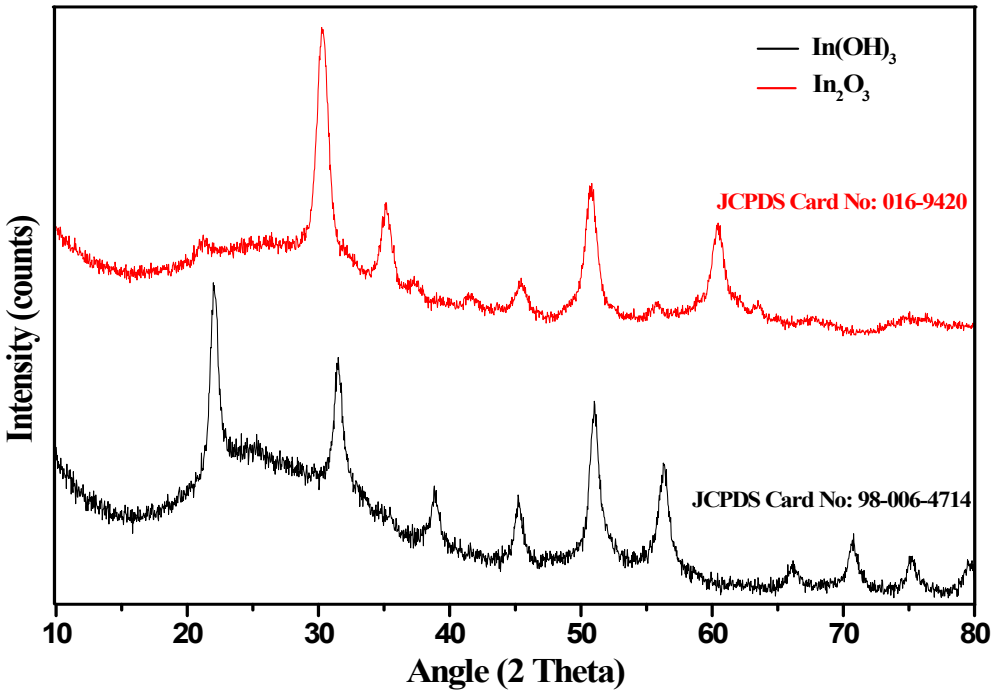

Figure S4: Powder X-ray diffraction patterns of $In(OH)_3$ and In_2O_3 NPs.

Photoluminescence Studies:

Since In_2O_3 belongs to transparent conducting oxide materials, the room temperature photoluminescence (PL) studies were also performed for both Au@In_2O_3 core shell and bare

In_2O_3 NPs under the excitation of 300 nm and shown in Figure S7. Normally the bulk In_2O_3 cannot emit visible light at room temperature.[2] However, The PL spectrum of In_2O_3 NPs (Figure S2) exhibited three emission bands at 428 (violet), 470 (blue), and 562 nm (green) whereas the Au@In_2O_3 core-shell NPs also exhibited three emission bands at 398, 425, and 470 nm in violet and blue regions respectively. The luminescent emission mechanism can be divided into two broad categories: near band edge (NBE) emissions and deep level (DL) emissions. NBE emissions can be favored by the high crystal quality and quantum confinement effect, and the DL emissions can be found due to impurities, low crystallinity or structure defects. In the case of In_2O_3 and Au@In_2O_3 core-shell NPs, the luminescence emission mechanism was attributed to the existence of oxygen vacancies. These oxygen vacancies can acts as deep defect donors in semiconductors and induce the formation of new energy levels in the bandgap.[3] The blue emission resulted from the radioactive recombination of a photo-excited hole and an electron occupying one of the oxygen vacancies.[3] The other visible emission bands observed in the spectra are related to different energy levels produced by the oxygen vacancies caused during calcination process[4] and these oxygen vacancies were confirmed by XPS studies in earlier section. However in the case of Au@In_2O_3 core-shell nanoparticles, the PL properties were weakened and some emission peaks disappeared, indicating that the energy band structures changed due to presence of extra Au metals. This type of quenching may come from luminescence reabsorption by the gold nanoparticles present in the Au@ In_2O_3 core-shell nanoparticles.[5]

Raman Studies:

The Raman spectrum of Au@In_2O_3 core-shell and In_2O_3 NPs are shown in Figure S8 together with their microstructural images. Since cubic In_2O_3 structure belongs to the I^3_a, T^1_h space group, [6] then the structure contains two kinds of cations: 8 In^{3+} with side symmetry S6 and 24 In^{3+} with point symmetry C2. The 48 oxygen atoms in the body-centered cell are on general positions (e) with C1 site symmetry. For such a structure, the following vibration modes are predicted[7]:

$$4A_g+4E_g+14T_g+5A_u+5E_u+16T_u$$

The vibrations with symmetry A_g, E_g, and T_g are Raman active and infrared inactive, while the T_u vibrations are infrared active and Raman inactive. The A_u and E_u vibrations are inactive in both infrared and Raman measurements. The peak at 121 cm^{-1} is assigned to the In-O vibration of InO_6 structure units.[8] The peak observed at 300 cm^{-1} is usually interpreted as the bending

vibration δ (InO_6) of octahedrons. The other two peaks 481 and 595 cm^{-1} are attributed to the stretching vibrations of the same ν (InO_6) octahedrons and these data was consistent with the earlier reports.[9, 10] Here is slight shift in the vibrational modes of Au@In_2O_3 core-shell NPs as compared to In_2O_3 modes which is due to the presence of extra foreign element in the core-shell NPs.

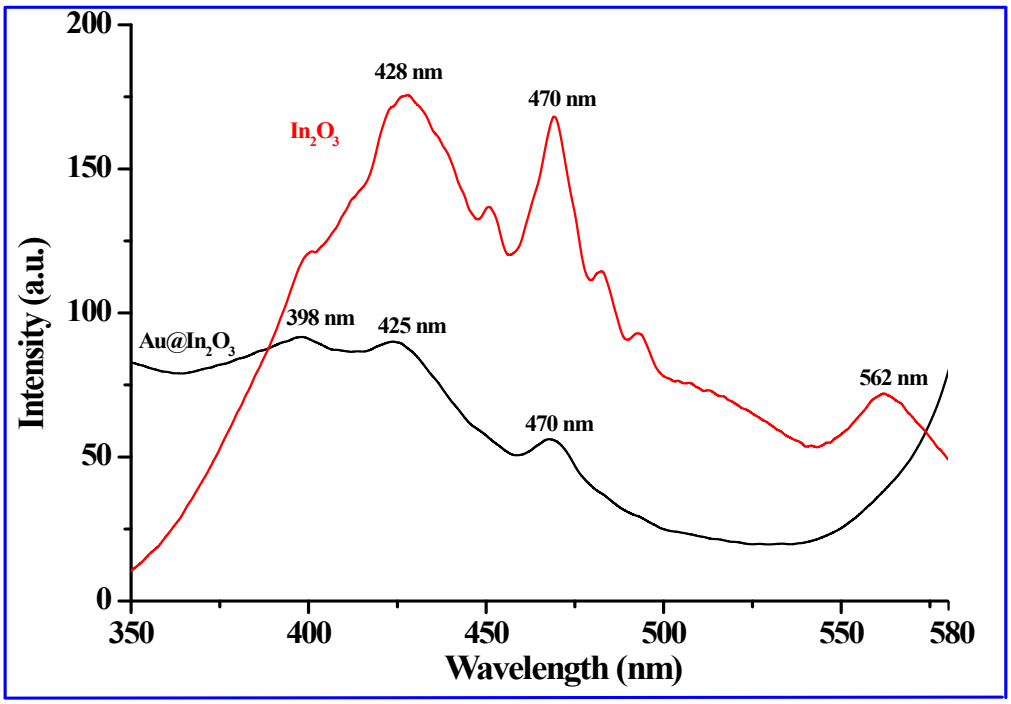

Figure S5: Photoluminescence spectra of Au@In_2O_3 core-shell and bare In_2O_3 NPs.

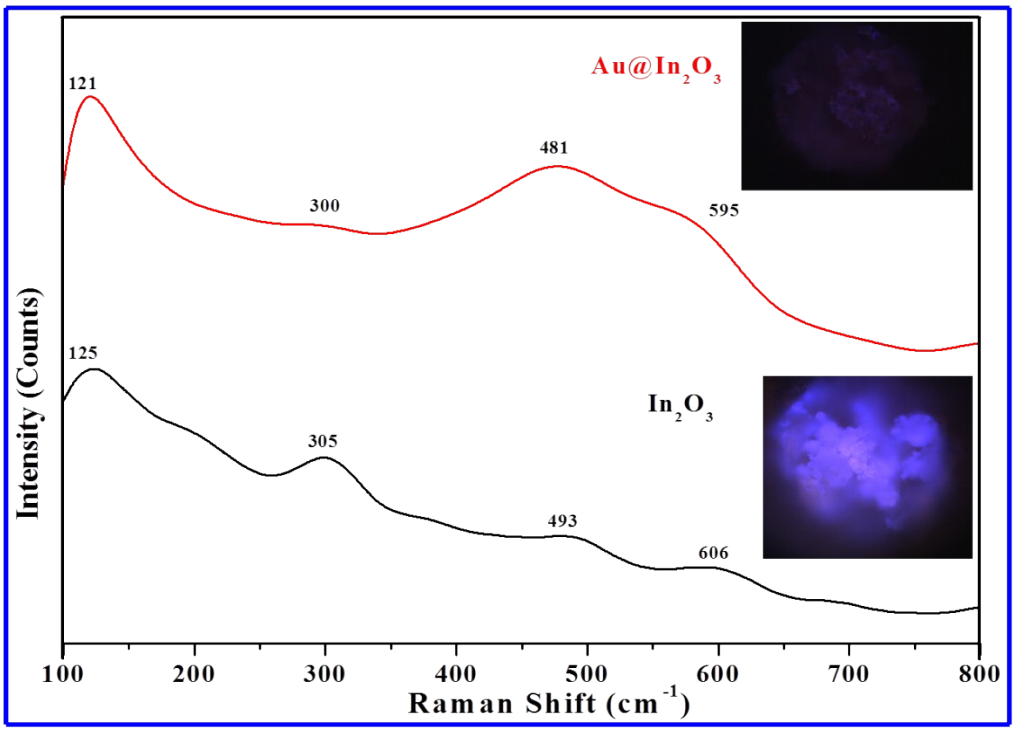

Figure S6: Raman Spectra of bare In_2O_3 and Au@In_2O_3 core-shell NPs with their microscopic surface sample images

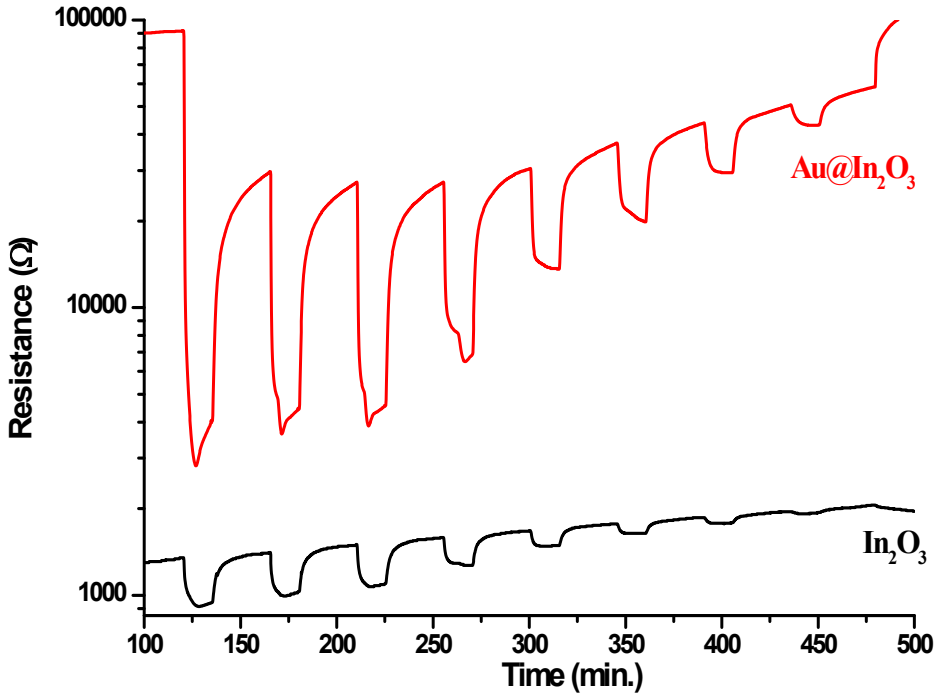

Figure S7: Resistance variation of $Au@In_2O_3$ core-shell and In_2O_3 NPs exposed to different H_2 gas concentrations at 200 ^oC.

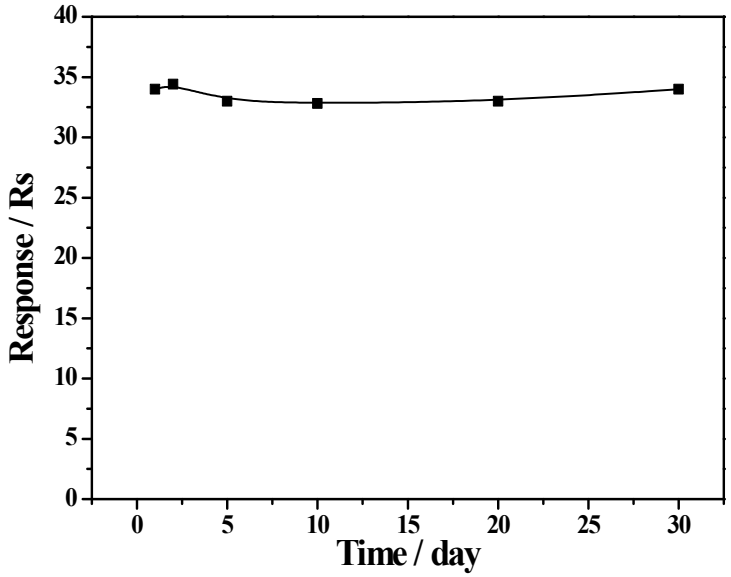

Figure S8: Long term stability of $Au@In_2O_3$ core-shell NPs at a working temperature of 300^oC to 100 ppm gas.

Tested Gas	Response Values	
	Au@In_2O_3 core-shell NPs sensor device	**In_2O_3 NPs sensor device**
H_2	**34.4**	**9.3**
CO	**6.4**	**5.2**
NO_2	**14.7**	**4.6**
Ethanol	**25.4**	**21**
Acetaldehyde	**21**	**20**

Table S1: Response values of Au@In_2O_3 core-shell and bare In_2O_3 NPs based sensor devices to 100 ppm to different gases at operating temperature of 300 ^oC.

References

(1) J. Zai, J. Zhu, R. Qi, X. Qiana, *J. Mater. Chem. A* 2013, **1**, 735-745.

(2) Ohhata, Y.; Shinoki, F.; Yoshida, S. Optical Properties of r.f. Reactive Sputtered Tin Doped In_2O_3 Films. *Thin Solid Films* **1979**, *59*, 255–261.

(3) Jin, L.- N.; Liu, Q.; Sun, W.- Y. Size-controlled Indium(III)–benzenedicarboxylate Hexagonal Rods and Their Transformation to In_2O_3 Hollow Structures. *Cryst. Eng. Commun.* **2013**, *15,* 4779-4784.

(4) Yu, D.B.; Yu, S.H.; Zhang, S.Y.; Zuo, J. Wang, D.B.; Qian, Y.T. Metastable Hexagonal In_2O_3 Nanofibers Templated from InOOH Nanofibers under Ambient Pressure. *Adv. Funct. Mater.* **2003**, *13,* 497-501.

(5) Bertry, L.; Durupthy, O.; Aschehoug, P.; Viana, B.; Chanéac, C. Experimental Evidence of Luminescence Quenching at Long Coupling Distances in Europium (III) Doped Core-Shell Gold Silica Nanoparticles. *Gold Bull.* **2013**, *46*, 349–355.

(6) Imai, H.; Tominaga, A.; Hirashima, H.; Toki, M.; Asakuma, N. Ultraviolet-reduced Reduction and Crystallization of Indium Oxide Films. *J. Appl. Phys.* **1999**, *85*, 203–208.

(7) Ferraro, J. R.; Nakamoto, K. *Introductory Raman Spectroscopy*; Academic Press: Boston, 1994.

(8) Zhu, H.; Wang, X. L.; Yang, F.; Yang, X. R. Template-Free, Surfactantless Route to Fabricate $In(OH)_3$ Monocrystalline Nanoarchitectures and Their Conversion to In_2O_3. *Cryst. Growth Des.* **2008**, *8*, 950–956.

(9) Gan, J.; Lu, X.; Wu, J.; Xie, S.; Zhai, T.; Yu, M.; Zhang, Z.; Mao, Y.; Wang, S. C.; Shen, Y.; Tong, Y. Oxygen Vacancies Promoting Photoelectrochemical Performance of In_2O_3 Nanocubes, *Sci. Rep.* **2013**, *3*, 1021.

(10) Kim, H. S.; Na, H. G.; Yang, J. C.; Lee, C.; Kim, H.W. Synthesis, Structure, Photoluminescence, and Raman Spectrum of Indium Oxide Nanowires. *Acta Phys. Pol. A* **2011**, *119*, 143-145.